

Microstructural Evaluation and Influence of Welding Parameters on Electrode Plunge Depth in Resistance Spot Welded Dissimilar DP800HF/1200M Steel Joints

^{1,4}Melih Kekik, ^{*2}Fatih Özen, ³Erdoğan İlhan, ⁴Salim Aslanlar

¹Ak-Pres A.Ş., 2. Organized Industrial Zone, Road No 2, No:20, Sakarya,

melih.kekik@akpres.com 

²Batman University, Faculty of Technology, Mechanical and Manufacturing Engineering Department, Batman,

fatih.ozen@batman.edu.tr 

³ Sakarya University of Applied Sciences, Adapazarı Vocational School, Department of Machinery and Metal Technologies,

Sakarya, eilhan@subu.edu.tr 

⁴Sakarya University of Applied Sciences, Faculty of Technology, Metallurgical and Materials Engineering, Sakarya,

aslanlar@subu.edu.tr 

Research Paper

Arrival Date: 12.01.2021

Accepted Date: 28.03.2021

Abstract

Advanced high strength steels (AHSS) are newly developed steels that has versatile mechanical properties. These steels enables to design low weight cars with high safety standards. Also, weight reduction in vehicles plays a significant role for saving fossil fuels which is limited and causes carbon emissions. Dual phase (DP) and Martensitic steels are prominent in AHSS family because they are inexpensive and has vast application areas. DP steels are used for general purpose applications and Martensitic steels are used for reinforcement parts in vehicles. In this study, high formable grade Dual phase steel with 800 MPa tensile strength and Martensitic steel with 1200 MPa tensile strength were welded with resistance spot welding technique which is the most widely practiced joining method in the industry. Electrode indentation depths, its effect on tensile-shear loads and microstructural characterizations were investigated. According to the results, the lowest tensile shear loads were acquired between both between 0-0.2 mm and between 0.85-1mm electrode plunge depths. Medial electrode plunge depths showed high tensile shear loads. Some welding defects were encountered including secondary phase formations, shrinkage voids, intergranular shrinkage gaps and vertical cracks in the weld nugget. It is find out that the weld defects were formed due to cooling gradient while solidifying, electrode force, and improper weld parameters.

Keywords: AHSS, Resistance spot welding, DP steels, Martensitic steels, Microstructure.

1. INTRODUCTION

Today, global warming, CO₂ emissions, the limit of fossil fuels and high oil prices are among the main factors affecting the whole world [1, 2]. Due to these difficulties, various weight reduction efforts have been initiated in the automotive industry without loss of safety [3]. The key role of weight reduction is developing new steels with high strength that ensures low weight designs for steel components. To achieve this goal, firstly, high strength low alloy (HSLA) steels have been developed. HSLA steels have moderate tensile strength with high ductility [4]. With further developments, advanced high strength steels have been developed. Based on design features, different steel grades of AHSS have been developed with a wide range of mechanical properties containing different microstructures [5]. Among AHSS steels, Dual Phase (DP) and Martensitic Steels (MS) steels have drawn attention in the automotive industry thanks to their unique mechanical properties and prices [6].

DP steels have high tensile strength up to 1000 MPa with good formability capabilities. They have martensite phase in ferrite matrix [7]. They are relatively cheap compared to other AHSS families thanks to both low cost processing operations and low cost constituents. They have different formability grades with high tensile strength. DP steels generally used for automotive chassis components. These steels have found large usage area in automotive industry [8].

Martensitic steels has similar microstructure with DP steels. They have also martensite phase in ferrite matrix. However, MS contains a high amount of martensite phase in ferrite matrix [9]. Thus, increasing tensile strength up to 1.7 GPa have been possible with low elongations [10, 11]. MS have been utilized for reinforcement and anti-intrusion parts that highly increases the safety [12, 13].

Resistance spot welding (RSW) is the most utilized welding method in manufacturing of automobiles especially for sheet components [14, 15]. An average automobile generally

*Corresponding Author: Batman University, Faculty of Technology, Mechanical and Manufacturing Engineering Department, Batman, e mail: fatih.ozen@batman.edu.tr, Telephone: +90 (488) 217 35 00

contains 3000-5000 spot welds [16]. The number of resistance spot welds on the automobile increases the health and importance of the joints.

Resistance spot welding is based on the compression of the metal sheets under a compression force with copper electrodes from both sides and then, the metal is melted with joule effect [17]. Electrode pressure and heat with a welding time forms the weld nugget. The weld nugget is formed between steel sheets where the highest electrical resistivity is constituted. Weld nugget diameter is also an indicator of weld reliability. Weld nugget diameter generally controls mechanical performance of RSW applied joints [18]. However, there is not a linear relationship between weld welding parameters, weld nugget diameter and mechanical performance of welding joint.

Another different aspect is electrode plunge depth. Electrode plunge depths with high amounts reduces aesthetic appearance and impedes it usage for visually remarkable parts [19]. In low electrode plunge depths, acquired with various current, welding time and electrode force, can causes low tensile-shear loads highly affecting mechanical performance of RSW applied joints [20].

In this work, effect of welding time and welding currents on electrode indentation depths of RSW applied dissimilar Martensitic/DP steel joints have been studied. Metallographic examinations were executed. MS grades having 1200 MPa tensile strength and DP steel having 1000 MPa tensile strength with high formability grade were used in experiments.

2. MATERIAL and METHOD

DP steel that belongs to high formability grade (DP1000HF) with 1.1-mm thickness and Martensitic steel (MS1200) with 1.2-mm thickness were acquired from local dealer. Their mechanical properties and chemical composition described by manufacturers are presented in Table 1 and Table 2, respectively.

Table 1. Chemical composition of DP800HF and MS1200 (wt.-%)

	C	Si	Mn	Al	Cr	Mo	Co
DP800HF	0.16	0.5	2.2	0.7	0.45	-	-
MS1200	0.07	0.20	1.6	0.03	0.01	0.03	0.013

Table 2. Mechanical properties of DP800HF and MS1200

	Yield strength [N/mm ²]	Tensile strength [N/mm ²]	Elongation [%]
DP800HF	532.9	920.7	16.7
MS1200	950	1282	3

Tensile-shear tests were carried out on the SHIMADZU AG-XD 50kN universal test device. Tensile speed was adjusted to 10-mm/min. The technical drawing of the tensile-shear test specimen is presented in Figure 1. Electrode plunge

depth (EPD) of both steels that measured for experiments is also presented in the figure. EPD of the RSW joints were measured with Nikon SMZ stereo microscope. The EPD measurements were performed prior to metallographic examinations.

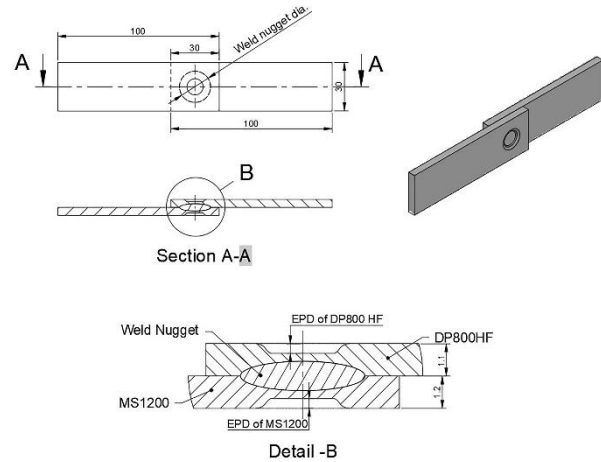


Figure 1. The technical drawing of resistance spot welded tensile-shear test specimen and details of EPD.

Before the experiment, all welding surfaces chemically and ultrasonically were cleaned to avoid dirt and oxides that could affect welding quality. Resistance spot welding machine having 120 kVA maximum capacity with pneumatically controlled jaws was used for experiments. The welding parameters were adjusted with HMI interface. Resistance spot welds were executed under 5 kN electrode force. Currents and welding times were constantly measured with Dengeshia (Japan) welding amperemeter. 6-mm tip diameter Cu-Cr electrodes with EN ISO5182 standard were used for experiments. The electrodes were cooled down with constant 6 L/min water flow. The holding times before and after welding operation were adjusted to 25 cycle (1 Cycle=0.02 s). Various welding durations and welding current combinations were utilized in experiments to see their effects separately. Welding currents and welding times used in experiments is presented in Table 3 with experiment sequence.

Table 3. Welding parameters and welding currents used in experiments with sequence.

	Welding durations (Cycle)					
	5	10	15	20	25	30
8.44	-	6	12	17	22	26
9.6	1	7	13	18	23	27
11.8	2	8	14	19	24	28
13.5	3	9	15	20	25	-
14.5	4	10	16	21	-	-
15.5	5	11	-	-	-	-

For SEM examinations, RSW applied joints were cut from centerline of the weld nugget. Conventional procedures were adopted for microstructural examinations. The weld joint was etched with %5 Nital solution for 5 s. JEOL JSM-5600 Scanning Electron Microscope (SEM) with Energy Dispersive x-ray Spectroscopy (EDS) was used for microstructural examination. The heat input that used in explanations is obtained from following equation;

$$Q = I^2 \cdot R \cdot t \tag{1}$$

Where, Q is Heat input (Joule), I is Ampere (A), R is total electrical resistance (Ω) and t is welding time (s).

3. RESULTS and DISCUSSION

3.1. Electrode Plunge Depth Behaviors

Effect of welding time and welding currents on EPD of DP800HF steel side of the RSW applied joint is presented in Figure 2. According to the figure, there is a linear relation between EPD and heat input. As the weld time increases, the ratio of EPD to weld current remains approximately constant. Namely, heat input increases the severity of EPD with the same trend. EPD of DP steel side shows the maximum plunge depths in 20 and 25 cycle welding times in 13.5 kA and 14.5 kA welding currents as 1-mm, respectively.

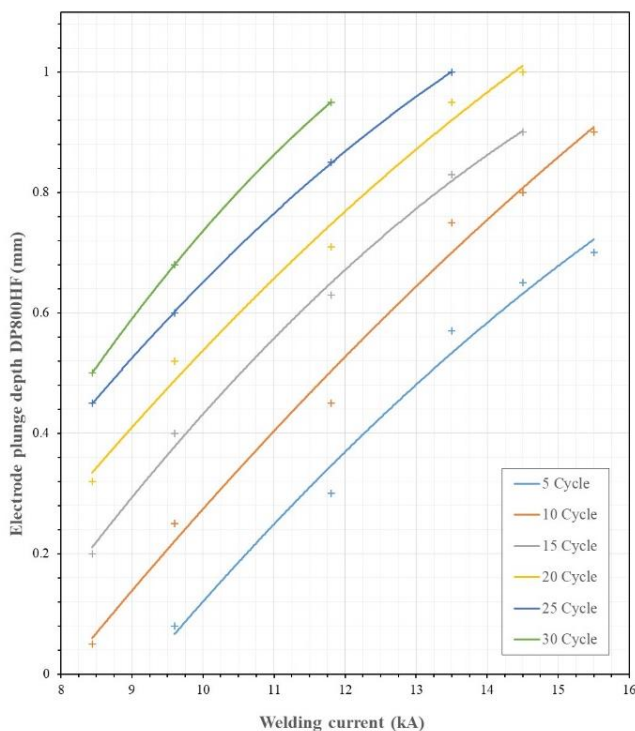


Figure 2. Electrode indentation depths of DP800HF steel side with respect to welding parameters.

EPD behavior of MS1200 steel against welding parameters is presented in Figure 3. EPD has similar characterizations with DP800HF steel. However, the maximum EPD for MS

was acquired in 30 cycle welding time and 11.75 kA welding current.

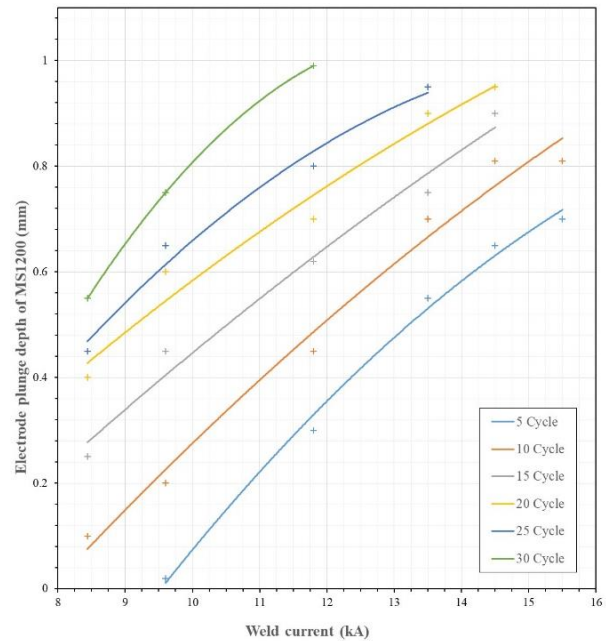


Figure 3. Electrode indentation depths of Martensitic steel side with respect to welding parameters.

When compared to DP800HF, EPD of MS1200 have a little bit lower but have similar characterization except for 20, 25 and 30 cycle welding times. In 20 and 25 cycle welding times, the maximum electrode plunge depths were obtained in DP800HF side. In 30 cycles welding time, there is a small deviation from each other that is acceptable for physical experiments. The main reason for lower EPD of MS1200 is attributed to the presence of high martensite ratio that has high much higher hardness than DP800HF.

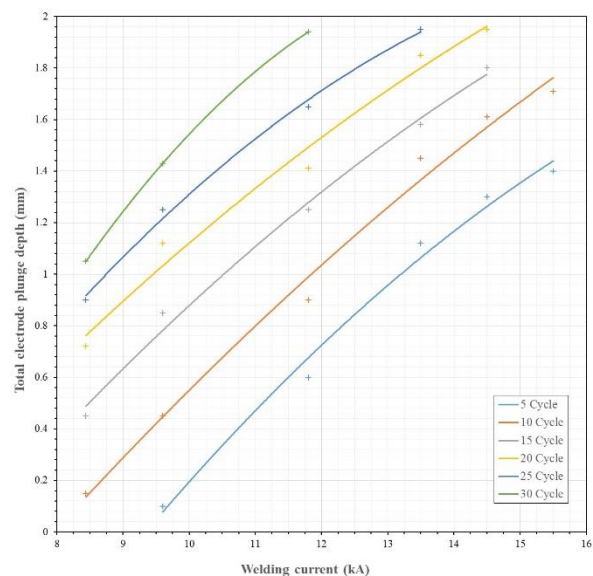


Figure 4. Electrode plunge depths of both sides with respect to welding parameters.

Total EPD was acquired with combination of both MS1200 and DP800HF is presented in Figure 4. The maximum electrode plunge depth for both steel was 1.96 mm. This climax point was achieved the highest currents of the 20, 25 and 30 cycle welding times. High EPD's of both sides at high heat inputs is an expected situation in the RSW method.

Effect of EPD for MS side and DP steel side on tensile-shear load is presented in Figure 5 and 6, respectively. According to results, the maximum tensile-shear load was acquired at 0.64 mm EPD of for MS side while 0.6 mm for DP steel side as 17960 N. MS showed similar characteristics with DP steel side on tensile shear load capacity with minimal deviations. The maximum deviation of EPD in both steels was below 0.1 mm. The lowest tensile-shear loads were achieved both between 0-0.2 mm and between 0.85-1mm. The low heat inputs were induced lower tensile-shear loads between 0-0.2 mm EPD while the high heat input presented in another low tensile-shear loads were between 0.85-1 mm EPD.

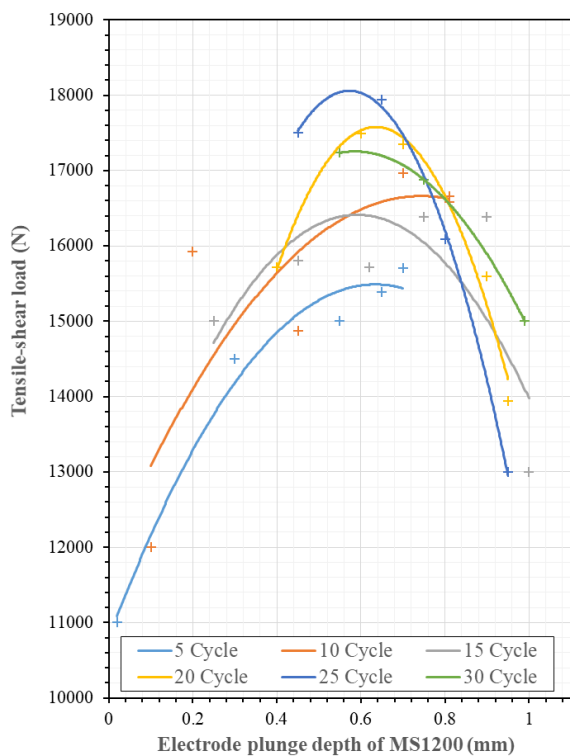


Figure 5. Tensile-shear load against electrode plunge depth of MS1200.

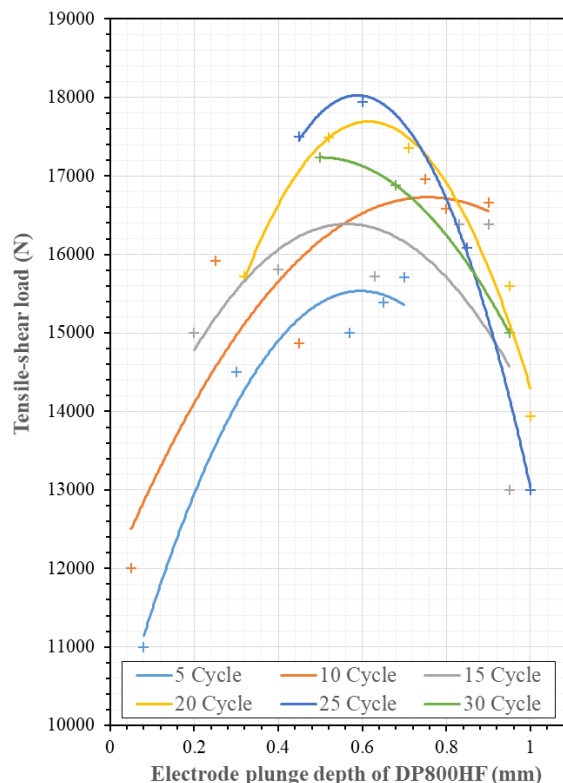


Figure 6. Tensile-shear load against electrode plunge depth of DP800HF.

3.2. Microstructural Characterizations

Microstructural graphs from weld nugget and heat affected zone (HAZ) of DP800HF/MS1200 RSW applied joint is presented in Figure 7 with different magnifications. According to figures, weld nugget zone has exact boundary from HAZ. Transition from HAZ to base materials (BM) illustrated with a black band that shows the end of the thermal transition. This transition between HAZ and BM has thicker characteristic in DP800HF steel side. The reason for this thickness is existence of higher amount ferrite that allowed much wider phase transition area due to its higher heat conductivity [21].

The weld nugget is mainly consists of lath martensite generated with thermal cooling gradient (Figure 7.d and 7.f). Weld nugget boundary shows fully melted and cooled region as shown in Figure 7.b. In this case, the thermal cooling gradient is start from weld nugget/HAZ frontier to the last solidifying region, namely, weld nugget center. During solidifying, heat is transferred from weld nugget to electrode that cooled with constant water flow. Therefore, the thermal cooling gradient was played an important role to form martensite that gradually coarsed towards weld nugget, but with preserving its natural orientation.

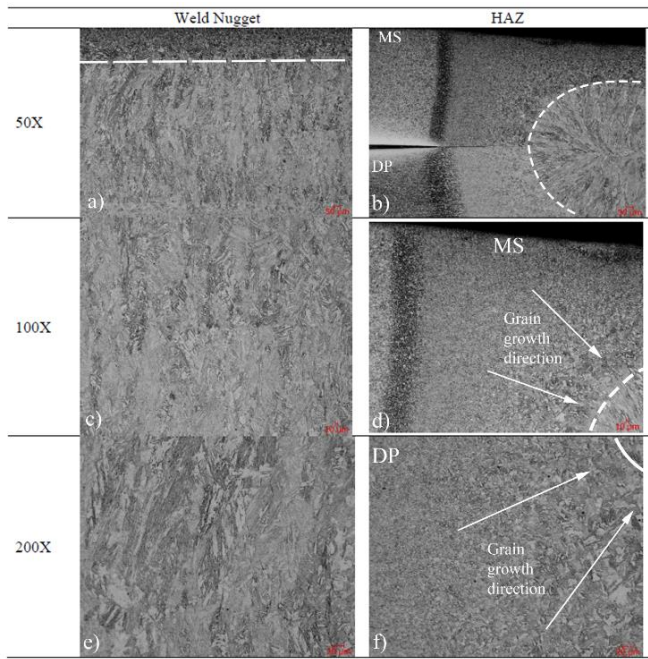


Figure 7. Microstructure of RSW applied DP800HF - MS1200 with different magnifications

Figure 8 shows SEM image from the focal point of thermal gradients in the weld nugget zone of spot welded DP800HF/MS1200 steel joint. According to micrograph, weld center was composed of lath martensite with small fractions of ferrite. The size of martensite is approximately between 40 and 60 μm while the size of the martensite in both steels from BM was between of 3-6 μm .

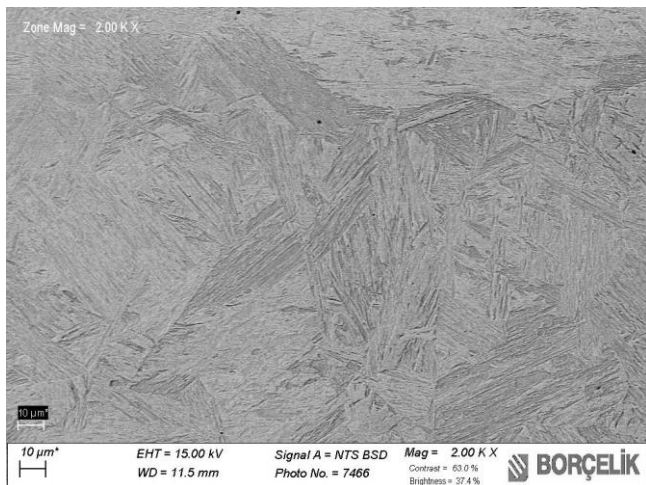


Figure 8. Weld nugget of the RSW applied DP800HF - MS1200.

Figure 9.a and 9.b shows a detailed graph from HAZ region of MS1200 and DP800HF steel, respectively. According to figures, coarsening of martensite laths toward weld nugget can easily be seen. However, the amount of ferrite zones that marked with white has different characterizations. In MS, the amount of martensite is far more than that of DP800HF. As for ferrite, a vice versa situation was occurred. The maximum amount of ferrite were formed in DP800HF. High

ferrite formation can be attributed to martensite fractions in steels before welding.

Similar microstructure characterizations were also coincided in the literature;

Pourvani et al. [22] studied the weldability of resistance spot welded 1200MS joint. They find out that heat affected zone were consisted of tempered coarsed martensite and ferrite. A single phase with lath martensite was formed in the weld nugget.

Di et al. [23] Investigated laser weldability of similar and dissimilar DP780 and DP980 steel joints. It is revealed that the weld nugget zone was formed with lath martensite for all DP joints. It is also described that the alloying elements was equally distributed in the weld nugget zone.

Bandyopadhyay et al. [24] studied microstructure and failure behavior of laser welded DP980 steels. Tempered martensite was formed at the heat affected zone and induced a soft region. This oft region reduced the formability of the welded blanks.

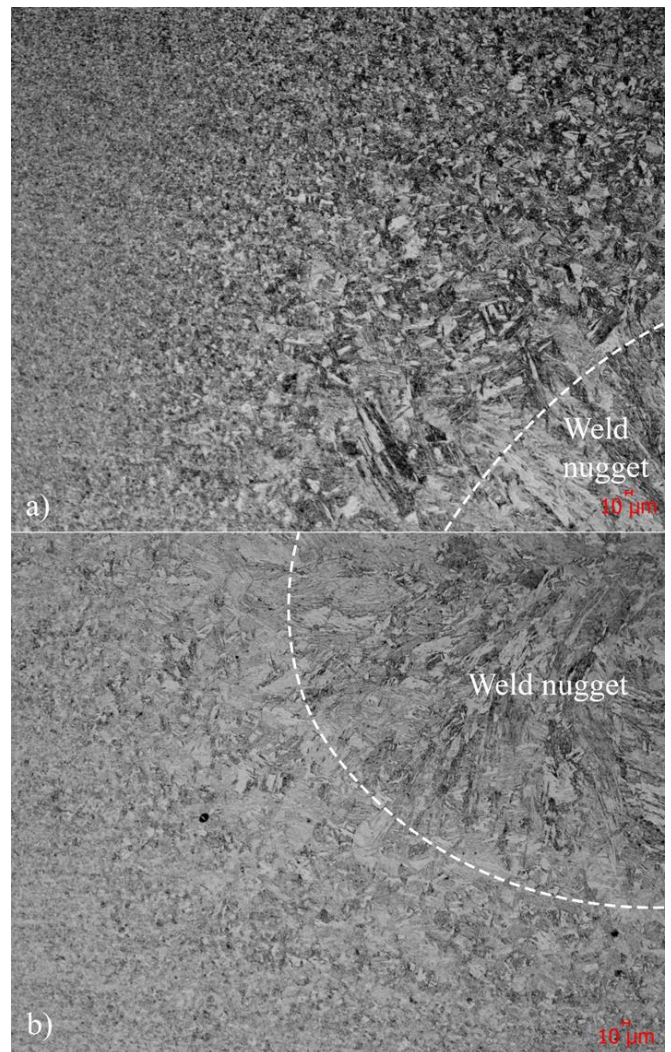


Figure 9. HAZ of a) MS1200 and b) DP800HF.

While welding of dissimilar MS1200/DP800HF steels, some defects were detected in microstructure. Figure 10 a-d shows encountered defects in welding of MS1200/DP800HF steels. According to micrographs, the defects were mainly formed in weld nugget zone. Cracks, secondary phase formations, shrinkage gaps were formed in weld nugget zone. The other defect that run into is Cu penetration in electrode contact surface.

Figure 10.a shows a shrinkage gap and secondary phase formation. This defect is situated at the center of the weld nugget zone. As soon as the weld nugget cools from the molten state, it commenced to solidify from the outer shell to inner regions. During the solidification, shrinkage is also taken place due to thermal contraction. The last place that solidifies is the focal point of the cooling gradients, namely, the horizontal centerline of the weld nugget.

Secondary phases that formed at the centerline of the weld nugget is a hint to low melting alloys. Normally, this low melting secondary phases is formed at the outer boundary of grains. However, gradual cool down of the grains caused accumulation of the secondary low melting phases at the center of the weld nugget because of the low solidification temperature.

The shrinkage in low severity caused intergranular voids and cracks at the center of the weld nugget. Figure 10.b shows intergranular gaps that resulted from insufficient volume due to thermal shrinkage. These gaps were formed both with partially vertical direction and with equiaxed direction.

In case of high electrode force, melted weld nugget was forced out of the separation surfaces of the sheets. Successive solidification and shrinkage has led to vertical cooling cracks as shown in Figure 10.c. These cracks were occurred between the grains, effectuating the weakest regions during cooling. Formation of the cracks, porosities and secondary alloys in welding of new generation steels were also reported in the literature;

Schmidová et al. [25] studied effect of Nb on the failure of dual-phase steel in dissimilar welds. Formation of porosities, cracks, and low melting secondary alloys in weld nugget was reported.

Wang et al. [26] studied resistance spot weldability of Q&P980 steels. They find out cracks and porosities in the weld nugget.

Another defect is penetration of electrode material into contact surface. Figure 10.d shows penetration of Cu from electrode/sheet contact surface. The detailed SEM image and EDS analysis were executed from penetrated metal is illustrated in Figure 11.a and 11.b, respectively. EDS analysis showed there is high amount of Cu with low amount of Fe (Table 4). This elemental measurement proves that the copper acquired from the electrode.

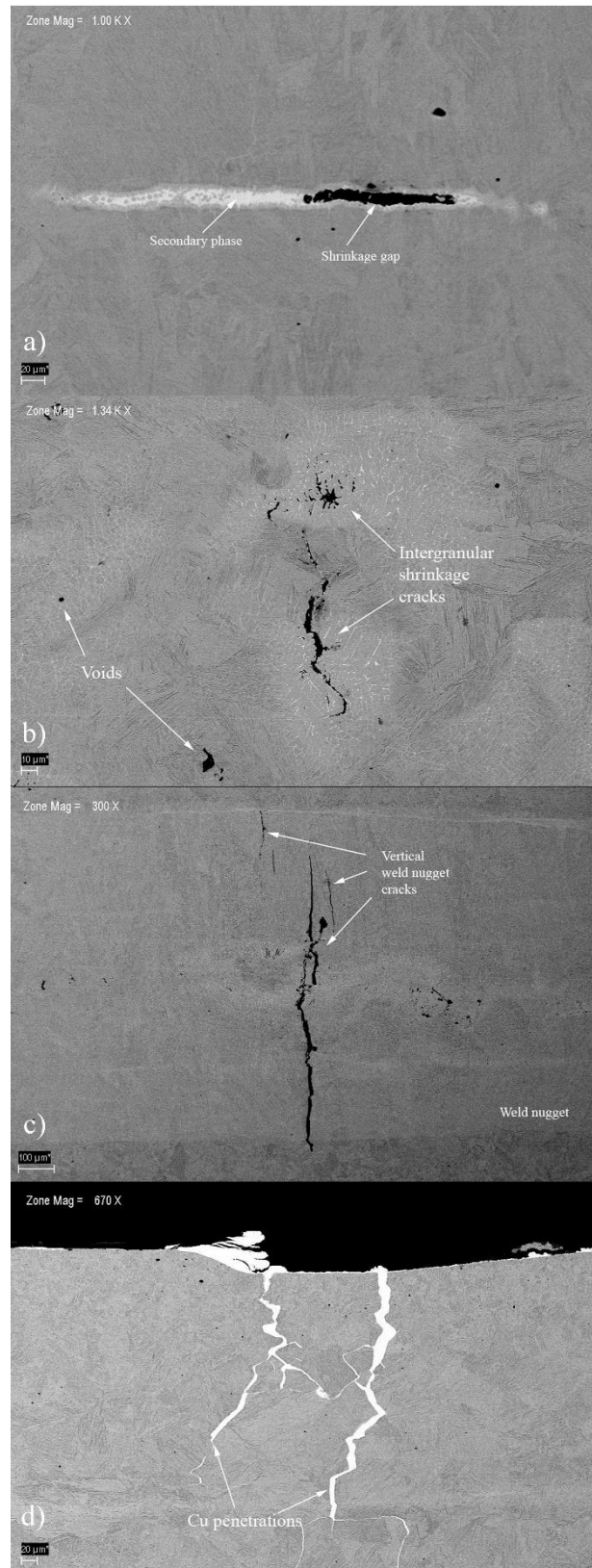


Figure 10. SEM micrographs of weld defects a) Shrinkage gap and secondary phase formation, b) Intergranular shrinkage cracks, c) Vertical weld nugget cracks and, d) Penetration of Cu from electrodes.

The penetration of Cu into intergranular gaps that formed during welding is somehow related to electrode softening and evaporation of surface material by high welding heat input induced by high welding current and welding. If there was a standard melting on electrode surface, there would be spills and residues on the contact surface of steel within a maximum of 30 cycle (0.6 seconds). However, the penetration from the surface of the material towards the inner regions can only be achieved with a pressure. It is an indication that the electrode material achieved to vapour phase locally by the applied heat in electrode tip. This evaporated Cu penetrated through intergranular gaps that is one of the easiest way to decrease vapour pressure and then Cu penetration between intergranular gaps is formed. It should be noted that the maximum resistance is achieved on the electrode surface of steels, but the second maximum resistances are achieved on electrode/steel contact surfaces.

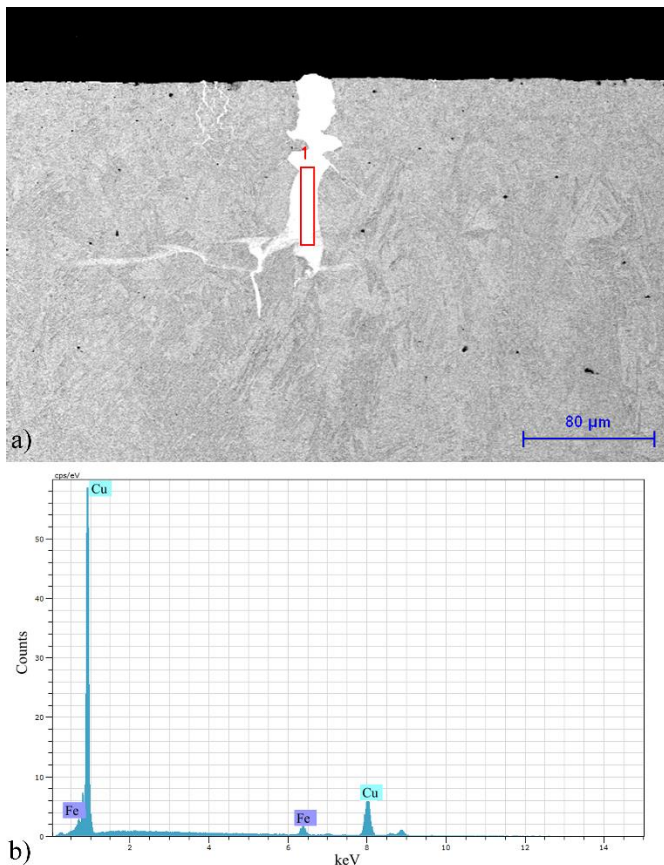


Figure 11. a) SEM micrograph of Cu penetration from electrodes, and b) its EDS results.

Table 4. EDS measurement result from penetration area.

Element	Wt.-%	Atomic (%)	Error (%)
Iron	6.80	7.83	0.3
Copper	91.03	92.17	3.0
Total	97.83	100.00	

4. CONCLUSIONS

A 800 MPa dual phase steel with high formability grade and 1200 MPa martensitic steel was welded successfully with

RSW technique. Electrode plunge depths and microstructural characterizations were examined. It is find out that the maximum tensile shear loads were achieved in moderate electrode plunge depths. Poor tensile shear loads were attained due to either insufficient or excess heat input that mirrors electrode plunge depths.

In microstructural investigations, heat induced defects such as shrinkage gaps or cracks and secondary phase formations were coincided in weld nugget. The main reason for secondary phases are gradual cooling down from outer shell to inner regions of weld nugget. Then the last solidifying low melting alloys were formed. Vertical cracks were also formed in the weld nugget due to softening and electrode application force while solidifying. Cu penetrations also formed on the contact surface due to excessive heat input. Cooling of electrodes was also played an important role in Cu penetrations. It is also determined that cooling of electrodes is of high importance while applying RSW technique.

Acknowledgements: The researchers are grateful to Borçelik steel company for providing access to the SEM device.

Author contributions: Concept – M.K., S. A.; Experiments and data collections &/or Processing – M.K., F. Ö. S.A.; Literature research – F.Ö, E.İ.; Writing and Review – F.Ö, M.K, S.A.

Conflict of Interest: No conflict of interest was declared by the authors.

Financial Disclosure: The authors declared that this study has received no financial support.

REFERENCES

[1] V. Behm et al., “Investigations on laser beam welding dissimilar material combinations of austenitic high manganese (FeMn) and ferrite steels” *Phys. Procedia*, vol. 56, no. C, pp. 610–619, 2014, doi: 10.1016/j.phpro.2014.08.049.

[2] S. Populoh, M. H. Aguirre, O. C. Brunko, K. Galazka, Y. Lu, and A. Weidenkaff, “High figure of merit in (Ti,Zr,Hf)NiSn half-Heusler alloys,” *Scr. Mater.*, vol. 66, no. 12, pp. 1073–1076, 2012, doi: 10.1016/j.scriptamat.2012.03.002.

[3] U. Özaraç, V. Onar, F. Özen, Y. S. Aslanlar, and N. Akkaş, “Effect of welding time on tensile-shear load in resistance spot welded TRIP 800 and microalloyed steels,” *Indian J. Chem. Technol.*, vol. 26, no. 4, pp. 355–357, 2019.

[4] N. Baluch, “Advanced High Strength Steel in Auto Industry : an Overview,” *Eng. Technol. Appl. Sci. Res.*, vol. 4, no. 4, p. 686, 2014.

[5] T. Depover, F. Vercruysse, A. Elmahdy, P. Verleysen, and K. Verbeken, “International Journal of Impact Engineering Evaluation of the hydrogen embrittlement susceptibility in DP steel under static and dynamic tensile conditions,” *Int. J. Impact Eng.*, vol. 123, no. March 2018, pp. 118–125, 2019, doi: 10.1016/j.ijimpeng.2018.10.002.

- [6] J. Liao, J. A. Sousa, A. B. Lopes, X. Xue, F. Barlat, and A. B. Pereira, "Mechanical, microstructural behaviour and modelling of dual phase steels under complex deformation paths," *Int. J. Plast.*, vol. 93, pp. 269–290, 2017, doi: 10.1016/j.ijplas.2016.03.010.
- [7] C. Landron, E. Maire, J. Adrien, H. Suhonen, P. Cloetens, and O. Bouaziz, "Non-destructive 3-D reconstruction of the martensitic phase in a dual-phase steel using synchrotron holotomography," *Scr. Mater.*, vol. 66, no. 12, pp. 1077–1080, 2012, doi: 10.1016/j.scriptamat.2012.03.003.
- [8] S. Pandre, V. Mhatre, N. Kotkunde, and S. Kumar, "Materials Today : Proceedings Strain hardening behavior of DP 590 steel using dislocation density based Kock-Mecking model," *Mater. Today Proc.*, no. xxxx, 2020, doi: 10.1016/j.matpr.2020.02.810.
- [9] V. H. L. Cortéz, F. A. R. Valdés, and L. T. Treviño, "Weldability of martensitic steel by resistance spot welding a neural network optimization in the automotive industry," *Mater. Manuf. Process.*, vol. 24, no. 12, pp. 1412–1417, 2009, doi: 10.1080/10426910903343916.
- [10] J. Venezuela, Q. Zhou, Q. Liu, M. Zhang, and A. Atrens, "Influence of hydrogen on the mechanical and fracture properties of some martensitic advanced high strength steels in simulated service conditions," *Corros. Sci.*, vol. 111, pp. 602–624, 2016, doi: 10.1016/j.corsci.2016.05.040.
- [11] J. Venezuela et al., "Further study of the hydrogen embrittlement of martensitic advanced high-strength steel in simulated auto service conditions," *Corros. Sci.*, vol. 135, no. January 2017, pp. 120–135, 2018, doi: 10.1016/j.corsci.2018.02.037.
- [12] S. Eva, C. Bohumil, and H. Petr, "Dynamic Fracture Behavior of the Martensitic High Strength Steel after Spot Welding," *Mater. Today Proc.*, vol. 3, no. 4, pp. 1156–1160, 2016, doi: 10.1016/j.matpr.2016.03.014.
- [13] M. Pouranvari and S. M. Mousavizadeh, "Failure mode of M130 Martensitic Resistance Spot Welds," *Mater. Tehnol.*, vol. 47, no. 6, pp. 771–776, 2013.
- [14] M. Huang, Q. Zhang, L. Qi, L. Deng, and Y. Li, "Effect of external magnetic field on resistance spot welding of aluminum alloy AA6061-T6," *J. Manuf. Process.*, vol. 50, no. January, pp. 456–466, 2020, doi: 10.1016/j.jmapro.2020.01.005.
- [15] K. Zhou and P. Yao, "Overview of recent advances of process analysis and quality control in resistance spot welding," *Mech. Syst. Signal Process.*, vol. 124, pp. 170–198, 2019, doi: 10.1016/j.ymsp.2019.01.041.
- [16] F. Hayat, "Effect of aging treatment on the microstructure and mechanical properties of the similar and dissimilar 6061-T6/7075-T651 RSW joints," *Mater. Sci. Eng. A*, vol. 556, pp. 834–843, 2012, doi: 10.1016/j.msea.2012.07.077.
- [17] X. Liu, S. Lan, and J. Ni, "Experimental study of Electro-Plastic Effect on Advanced High Strength Steels," *Mater. Sci. Eng. A*, vol. 582, pp. 211–218, 2013, doi: 10.1016/j.msea.2013.03.092.
- [18] F. Badkoobeh, A. Nouri, H. Hassannejad, and H. Mostaan, "Microstructure and mechanical properties of resistance spot welded dual-phase steels with various silicon contents," *Mater. Sci. Eng. A*, vol. 790, no. June, p. 139703, 2020, doi: 10.1016/j.msea.2020.139703.
- [19] D. Bračun, I. Polajnar, and J. Diaci, "Indentation shape parameters as Indicators of spot weld quality," *Int. J. Mater. Prod. Technol.*, vol. 27, no. 3–4, pp. 247–257, 2006, doi: 10.1504/IJMPT.2006.011275.
- [20] T. Khuenkaew and K. Kanlayasiri, "Selection of electrode tips for the resistance spot welding of dissimilar stainless steels," *MATEC Web Conf.*, vol. 192, pp. 1–4, 2018, doi: 10.1051/mateconf/201819201007.
- [21] J. Wilzer, F. Lüdtkke, S. Weber, and W. Theisen, "The influence of heat treatment and resulting microstructures on the thermophysical properties of martensitic steels," *J. Mater. Sci.*, vol. 48, no. 24, pp. 8483–8492, 2013, doi: 10.1007/s10853-013-7665-2.
- [22] M. Pouranvari, S. Sobhani, and F. Goodarzi, "Resistance spot welding of MS1200 martensitic advanced high strength steel: Microstructure-properties relationship," *J. Manuf. Process.*, vol. 31, pp. 867–874, 2018, doi: 10.1016/j.jmapro.2018.01.009.
- [23] H. Di, Q. Sun, X. Wang, and J. Li, "Microstructure and properties in dissimilar/similar weld joints between DP780 and DP980 steels processed by fiber laser welding," *J. Mater. Sci. Technol.*, vol. 33, no. 12, pp. 1561–1571, 2017, doi: 10.1016/j.jmst.2017.09.001.
- [24] K. Bandyopadhyay, S. K. Panda, P. Saha, V. H. Baltazar-Hernandez, and Y. N. Zhou, "Microstructures and failure analyses of DP980 laser welded blanks in formability context," *Mater. Sci. Eng. A*, vol. 652, pp. 250–263, 2016, doi: 10.1016/j.msea.2015.11.091.
- [25] E. Schmidová, M. R. Sunil Kumar, M. Schmid, and F. Bozkurt, "Role of Nb in the failure of dual-phase steel in heterogeneous welds," *Eng. Fail. Anal.*, vol. 116, no. July, 2020, doi: 10.1016/j.engfailanal.2020.104708.
- [26] B. Wang et al., "Investigation on fatigue fracture behaviors of spot welded Q&P980 steel," *Int. J. Fatigue*, vol. 66, pp. 20–28, 2014, doi: 10.1016/j.ijfatigue.2014.03.004.